AIP | The Journal of Chemical Physics

A configurational study of helium clusters doped with He^{*-} and He_2^{*-}

Rocío Rodríguez-Cantano, Tomás González-Lezana, Pablo Villarreal, and Franco A. Gianturco

Citation: The Journal of Chemical Physics **142**, 104303 (2015); doi: 10.1063/1.4913958
View online: http://dx.doi.org/10.1063/1.4913958
View Table of Contents: http://scitation.aip.org/content/aip/journal/jcp/142/10?ver=pdfcov
Published by the AIP Publishing

A configurational study of helium clusters doped with He^{*-} and He_2^{*-}

Rocío Rodríguez-Cantano,[1] Tomás González-Lezana,[1,a)] Pablo Villarreal,[1] and Franco A. Gianturco[2]
[1]*Instituto de Física Fundamental, CSIC, Serrano 123, 28006 Madrid, Spain*
[2]*Institute of Ion Physics, The University of Innsbruck, Technikerstr. 25, 6020 Innsbruck, Austria and Scuola Normale Superiore, Piazza dei Cavalieri 7, 56126 Pisa, Italy*

(Received 17 December 2014; accepted 11 February 2015; published online 9 March 2015)

Helium clusters doped with electronically excited atomic and molecular helium anions He^{*-} and He_2^{*-} at $T = 0.4$ K are studied by means of path integral Monte Carlo calculations. Geometry and energetics of the systems with up to 32 solvating He atoms are characterised. The interactions between the anions and the neutral He atoms have been described by fitting previously reported *ab initio* points to analytical expressions. The He_N–He^{*-} clusters with $N > 6$ display a structure defined by a bipyramid which completely solvates the atomic anion, whereas the rest of surrounding He atoms form a dimple around that initial cage. On the contrary, the structures observed for the He_N–He_2^{*-} clusters clearly show the dopant located outside the helium droplet, thereby confirming the heliophobic character of He_2^{*-}. © *2015 AIP Publishing LLC.* [http://dx.doi.org/10.1063/1.4913958]

I. INTRODUCTION

Among the most commonly investigated species embedded in helium droplets at low temperatures, charged atomic and molecular systems have received attention over the past years. In particular, besides the attachment of free electrons into large clusters, atomic and molecular He anions have been found to play a relevant role as charge carriers within this superfluid-like medium. Indications regarding the formation of negative He ions were inferred from the resonance-like profiles of the signal registered in crossed beam scattering experiments with supercritical liquid free jet expansions.[1] The excitation to metastable electronic states of the helium clusters was taken as the main mechanism producing He anions instead of direct interaction of electrons with the neutral He droplet.[1–3] In fact it is now well accepted that the process which leads to the formation of atomic helium anions is the result of a two-step reaction. First, the electron penetrating inside the helium droplet excites a He atom from the ground electronic state $He(1s^2\ ^1S)$ to its first excited state $He(1s2s\ ^3P)$, namely, He^*. The initial kinetic energy of the electron, ~22 eV, accounts both for the required penetration energy (1.2 eV)[4] and the excitation energy to obtain He^* (19.8 eV). Both the resulting zero kinetic energy electron and the excited He^* lie in separate bubbles within the helium environment[2,5–7] and finally combine to form He $(1s2s2p\ ^4P)$ He^{*-}, a fast ion which was initially observed in bulk helium as reported in Ref. 8.

The precise pathway which leads to the formation of the molecular anion $He_2(1\sigma_g^2 1\sigma_u 2\sigma_g\ ^1\pi_4\ ^4\Pi_g)$, hereafter He_2^{*-}, is however still subject of discussion. The process is not result of the dimerization of a He ground state atom and He^* or He^{*-} due to the presence of barriers which cannot be overcome at the low temperature of the helium droplets. The only two excited states of He capable to conduct a barrier-free dimerization with a ground state He are $He(1s2p\ ^3P)$ and $He(1s3p\ ^3P)$.[2] The above mentioned electron energy required to penetrate the helium droplet summed to the corresponding excitation energies lead to estimates for the formation energy of He_2^{*-} of 22.1 eV and 24.2 eV, respectively.[2,3]

Both species He^{*-} and He_2^{*-} show different behaviour once they become embedded in the droplet. On one hand, the atomic anion is highly mobile through the surrounding helium environment and has been suggested as the effective charge carrier in the formation of anions inside helium droplets instead of the previously assumed possibility of an electron bubble migrating to the dopant.[9,10] He^{*-} is also heliophilic since the process of surrounding the atomic anion with ground state He atoms is almost 3 times more favourable than the formation of a repulsive void around it.[2] The trend is completely the opposite for He_2^{*-} which is supposed to migrate to the surface of the helium droplet.

In addition to previous theoretical studies on the metastable states of both atomic and diatomic helium,[11] the interaction of He^{*-} and He_2^{*-} with He atoms has been recently investigated by means of quantum mechanical (QM) calculations of the coupled cluster with single, double and (perturbative) triple excitations CCSD(T) type.[5] *Ab initio* energies for the $He(^1S)$–$He^{*-}(^4P)$ and $He(^1S)$–$He_2^{*-}(^4\Sigma_g)$ interactions were calculated for different interparticle distances and angular orientations. The effect of the two anionic species on the helium environment and on immersed species was analysed by means of different structural and energetic quantities. The authors of Ref. 5 confirmed the main role played by He^{*-}, which remains inside the droplet, in the ionization of impurities embedded in the helium cluster and the difficulties for He_2^{*-} to interact with the dopant.

In this paper, we address the study of helium droplets He_N doped with the above mentioned anionic helium species with N ranging between 1 and 32 at $T = 0.4$ K by means of path integral Monte Carlo (PIMC) calculations. The differences in

a)Electronic mail: t.gonzalez.lezana@csic.es

the interaction between the He atoms and the He^{*-} and He_2^{*-} impurities, described via the analytical fitting of the *ab initio* points of Ref. 5, is expected to play a role in the structure and energetics of the doped helium aggregates. In a similar manner as in previous investigations on He_N–Ca,[12] He_N–Cs_2[13] or He_N–Rb_2,[14,15] the study of small and intermediate clusters provides useful insights regarding the intrinsic features of the interaction between dopant and solvent in larger droplets or bulk helium. The geometry and energetics of the clusters have been analyzed in terms of the number of the He atoms by means of the PIMC approach. This paper is structured as follows: In Sec. II, we present the theory of the method and describe the potential energy surface (PES) employed in the calculation; in Sec. III, results are shown and discussed in Sec. IV. Finally, conclusions are presented in Sec. V.

II. THEORY

A. Path integral Monte Carlo method

A full description about the PIMC method can be found in previous works,[14,16–18] so here we will only refer to the most relevant details. According to this approach, the thermal average of a quantum observable $\hat{A}$ is obtained as

$$\hat{A} = Z^{-1} \int d\mathcal{R} d\mathcal{R}' \rho(\mathcal{R}, \mathcal{R}'; \beta) \langle \mathcal{R} | \hat{A} | \mathcal{R}' \rangle, \tag{1}$$

where the density matrix at a temperature T, defined as $\rho(\mathcal{R}, \mathcal{R}'; \beta) = \langle \mathcal{R}' | e^{-\beta \hat{H}} | \mathcal{R} \rangle$, can be replaced by the product of M density matrices at a higher-temperature $T' = T \times M$ as follows:

$$\rho(\mathcal{R}_0, \mathcal{R}_M; \beta) = \int d\mathcal{R}_1 \dots d\mathcal{R}_{M-1} \prod_{k=0}^{M-1} \rho(\mathcal{R}_k, \mathcal{R}_{k+1}; \tau). \tag{2}$$

In Eq. (1), Z is the partition function and $\beta = 1/k_B T$. We have defined the discrete-time path as $\tau = \beta/M$, the time step of the path integral. $\mathcal{R}_k$ corresponds to the position vectors of the $\mathcal{N}$ particles of the system: $\mathcal{R}_k \equiv \{\mathbf{r}_1^k, \dots, \mathbf{r}_{\mathcal{N}}^k\}$. In the case of He_N–He^{*-}, $\mathcal{N}$ includes the N He atoms plus the atomic anion impurity, but for the diatomic anion, the impurity has been considered as fixed at the origin.

In order to take into account the bosonic character of the ^{4}He atom, the density matrix is symmetrized by summing over all permutations $\mathcal{P}$ of the particle labels[17]

$$\rho_B(\mathcal{R}, \mathcal{R}'; \beta) = \frac{1}{N!} \sum_{\mathcal{P}} \rho(\mathcal{R}, \mathcal{P}\mathcal{R}'; \beta). \tag{3}$$

The sampling procedure for the multislice many-particle movements is the multilevel Metropolis method,[16,19,20] with 8 beads involved in each Monte Carlo (MC) step. Analogously, up to 4 He atoms are allowed to take part in the exchange permutation sampling, a value tested for both pure and doped helium clusters.[16,21]

The total Hamiltonian $\hat{H}$ is written as follows:

$$\hat{H} = \hat{T}_X - \frac{\hbar^2}{2m_{\mathrm{He}}} \sum_{i=1}^{N} \nabla_i^2 + \sum_{i=1}^{N} V_{\mathrm{He-X}}(\mathbf{r}_i) + \sum_{i<j}^{N} V_{\mathrm{He-He}}(r_{ij}), \tag{4}$$

where $\hat{T}_X$ is the kinetic operator for the impurity X (taken as zero for the case of the non-moving He_2^{*-} case); m_{He} is the helium atom mass; $\mathbf{r}_i$ is the position vector of the ith He atom with respect to the dopant, or in case of a molecular species, with respect to its center of mass (CM), and $r_{ij} = |\mathbf{r}_i - \mathbf{r}_j|$ are helium-helium distances.

For the PIMC calculation, we have chosen the so-called *thermodynamic* estimator developed by Baker,[22] expressed as

$$E_T = \frac{3(\mathcal{N}-1)}{2\tau} - \left\langle \sum_{k=0}^{M-1} \sum_{i=1}^{N} \frac{(\mathbf{r}_i^k - \mathbf{r}_i^{k+1})^2}{4M\lambda\tau^2} - \frac{1}{M} \sum_{k=0}^{M-1} V(\mathcal{R}_k) \right\rangle, \tag{5}$$

where $\langle\rangle$ means averaging over the MC steps, and for the definition of $\lambda = \hbar^2/2m_{\mathrm{He}}$, we have considered that the mass is the same for both dopant and solvent, since this term vanishes for the case of the diatomic anion. The first term refers to the classical kinetic energy multiplied by the number of beads M and vanishes in the case of the molecular impurity. The second term accounts for the QM energy due to the spring-like interaction assumed between consecutive beads in the same ring describing a specific particle. This contribution becomes zero for the dopant assumed as fixed to the origin. The last sum contains the potential energy as specified in the last two terms of Eq. (4).

The low temperature considered in the calculations, $T = 0.4$ K, should not induce too much thermal excitation to the movement of the atoms constituting the cluster. Therefore, no confinement has been imposed to prevent any possible evaporation from the droplet. The number of beads M considered in the PIMC calculation varies between 50 and 500. In some cases, we will consider a classical version of this approach for $M = 1$, hereafter referred as classical MC (CMC). The average energy for each He_NX system considered here is finally obtained by extrapolating τ to 0 (that is, M to ∞) following a parabolic law.[13,23,24] The initial configurations of the PIMC simulations are taken from the geometries obtained by means of the CMC calculation. These, in turn, are the result of optimizations from the structures obtained from the exploration of the PES in search for the absolute minima performed with an evolutive algorithm (EA).[25] The calculations involve between 10^6 and 10^8 MC steps depending on the size of the cluster under study.

As in previous works on doped helium clusters,[13] information regarding the structure and geometry of the corresponding clusters can also be obtained by means of the radial probability density function for the He–He distance

$$\mathcal{D}_N(r_{\mathrm{He-He}}) = \frac{2}{N(N-1)M} \left\langle \sum_{k=0}^{M-1} \sum_{i<j}^{N} \delta(r_{\mathrm{He-He}} - r_{ij}^k) \right\rangle \tag{6}$$

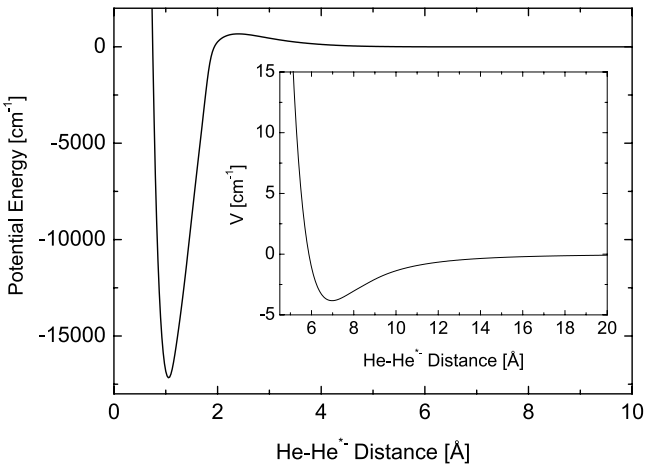

FIG. 1. Potential energy for He–He^{*-} obtained with the numerical fit of Eq. (10) for the *ab initio* points of Ref. 5. The inset amplifies the region of the secondary well. See text for details. Units for the energy are cm^{-1} and distances are measured in Å.

and for the distance between the He and the dopant impurity as follows:

$$\mathcal{D}_N(r_{\text{He-imp}}) = \frac{1}{NM}\left\langle \sum_{k=0}^{M-1}\sum_{i=1}^{N} \delta(r_{\text{He-imp}} - |\,\mathbf{r}_i^k\,|)\right\rangle. \quad (7)$$

Analogously, the angular distribution for $\cos\gamma$, with γ the angle formed between two He position vectors $\mathbf{r}_i^k$ and $\mathbf{r}_j^k$, is calculated as

$$\mathcal{D}_N(\cos\gamma) = \frac{2}{N(N-1)M}\left\langle \sum_{k=0}^{M-1}\sum_{i<j}^{N} \delta(\cos\gamma - |\,\mathbf{r}_i^k\cdot\mathbf{r}_j^k\,|)\right\rangle, \quad (8)$$

and, in the case of a diatomic impurity, such as He_2^{*-}, the distribution corresponding to $\cos\theta$, with θ describing the angle formed between the position vector of one He atom, $\mathbf{r}_i^k$, and the diatom axis, can be written as

$$\mathcal{D}_N(\cos\theta) = \frac{1}{NM}\left\langle \sum_{k=0}^{M-1}\sum_{i=1}^{N} \delta(\cos\theta - \cos\theta_i)\right\rangle. \quad (9)$$

B. Interaction potentials

As expressed in Eq. (4), the total potential is written as the sum of the corresponding pairwise He–He and He–anion interactions. The $V_{\text{He-He}}(r_{ij})$ interaction was described using the potential by Aziz and Slaman[26] with a well depth of ~7.59 cm^{-1} and a equilibrium distance of ~2.97 Å. For the potential between the helium atoms and the corresponding impurity, either the atomic anion, He^{*-}, or the diatomic anion, He_2^{*-}, numerical fits to the values reported in the QM CCSD(T) study of Ref. 5 were employed.

In particular, for the $V_{\text{He-He}^{*-}}$ case, the *ab initio* points reported by Huber and Mauracher[5] described four different regions. As shown in Fig. 1, there is a deep potential well of about ~17 000 cm^{-1} at r = 1.06 Å (region I), followed by a barrier with a maximum value located around ~2.2 Å (region II) which leads to a extremely shallow well (about ~3.8 cm^{-1}) at $r \sim 7$ Å (region III). Finally, region IV corresponds to the asymptotic behaviour which may be simulated by means of the corresponding ion-induced dipole interaction. The analytical expression for the complete fit of the *ab initio* points was thus the following:

$$V_{\text{He-He}^{*-}}(r) = (1 - g_4(r))\,\mathcal{F}_{\text{III}}(r) + \frac{c_4 g_4(r)}{r^4}, \quad (10)$$

where $c_4 = -13\,683.2521$ Å^{-4} cm^{-1} and

$$\mathcal{F}_{\text{III}}(r) = \mathcal{F}_{\text{II}}(r)\,(1 - g_3(r)) + g_3(r) f_3(r), \quad (11)$$

where

$$\mathcal{F}_{\text{II}}(r) = (1 - g_2(r))\,\mathcal{F}_{\text{I}}(r) - g_2(r) f_2(r), \quad (12)$$

with

$$\mathcal{F}_{\text{I}}(r) = (1 - g_1(r))\, f_1(r) + g_1(r) g_0(r). \quad (13)$$

In the above equations (10)–(13), we have defined

$$f_j(r) = D_j e^{-\tilde{\alpha}_j(r-\bar{r}_j)}\left(e^{-\alpha_j(r-\bar{r}_j)} - 2\right), \quad (14)$$

$$g_j(r) = \frac{a_j}{2}\left(1 + tanh\left[\beta_j(r - \bar{x}_j)\right]\right) - b_j, \quad (15)$$

with values for the corresponding parameters given in Table I.

The root-mean-square (rms) for the fit of the *ab initio* points to the analytical expression (10) is 10 cm^{-1}. Most of this deviation comes from the region I of the potential at both the repulsive component at very short He–impurity distances (where the *ab initio* points can range between 30 000 and 80 000 cm^{-1}) and the minimum of the deep potential well (≈−17 000 cm^{-1}), with specific values for the rms of up to 41 cm^{-1}. At the other regions, the situation becomes much less dramatic with a noticeable reduction of the deviation between the fit and the actual calculated points of less than 1.1 cm^{-1}.

TABLE I. Parameters for the interaction potential $V_{\text{He-He}^{*-}}(r)$ between the He atoms and the atomic anion, He^{*-}, defined in Eqs. (10)–(15).

	$j=0$	$j=1$	$j=2$	$j=3$	$j=4$
D_j (cm^{-1})		17 109.4319	668.0	3.82	
α_j (Å^{-1})		2.2202	2.1612	0.6330	
$\tilde{\alpha}_j$ (Å^{-1})		2.2202	1.4313	0.6330	
$\bar{r}_j$ (Å)		1.06	2.40	6.97	
a_j (cm^{-1})	22 367.3596	1	1	1	1
b_j (cm^{-1})	20 533.7740	0	0	0	0
β_j (Å^{-1})	2.1751	11.1642	9.6603	1.7588	2.0478
$\bar{x}_j$ (Å)	1.4816	1.1312	1.8168	4.1645	8.2767

TABLE II. Values of the $a_{\ell n}$ coefficients for the expansion in Eq. (17) for the $V_{\mathrm{He–He}_2^{*-}}(r,\cos\theta)$ potential describing the interaction between the diatomic anion impurity He_2^{*-} and the He atoms. See text for details.

	$n=0$	$n=1$	$n=2$	$n=3$	$n=4$	$n=5$
a_{n5} (10^7 Å^{-5} cm^{-1})	0.2055	0.1190	−1.2209	3.0799	−3.8827	1.7342
a_{n6} (10^9 Å^{-6} cm^{-1})	−0.0904	−0.0417	0.4457	−1.0453	1.2853	−0.5639
a_{n7} (10^{10} Å^{-7} cm^{-1})	0.1181	0.0494	−0.5404	1.2033	−1.4418	0.6200
a_{n8} (10^{10} Å^{-8} cm^{-1})	−0.4109	−0.1964	2.1065	−4.6991	5.4955	−2.3137

The interaction potential between the He atoms and the diatomic anion He_2^{*-} depends in turn both on the distance $r_{\mathrm{He–Imp}}$ and on the angle θ formed between the position vector of the He atom and the bond direction within the He_2^{*-} impurity

$$V_{\mathrm{He–He}_2^{*-}}(r,\cos\theta)=\begin{cases}\sum_{n=4}^{8} C_n(\cos\theta)/r^n & r>r_0\\ \sum_{n=4}^{8} C_n(\cos\theta)/r_0^n & r\le r_0\end{cases} \quad (16)$$

with a cutoff value of $r_0 = 6$ Å and where

$$C_n(\cos\theta)=\begin{cases}-C_4 & n=4\\ \sum_{\ell=0}^{5} a_{\ell n}\cos^{\ell}\theta & n>4\end{cases}, \quad (17)$$

where $C_4 = 11\,363.2878$ Å^{-4} cm^{-1}. Table II shows the values of the corresponding parameters in the expansion of Eq. (17). The interparticle distance within the He_2^{*-} unit is taken as the corresponding to the minimum of the He–He* potential, ∼1.2 Å (see Fig. 1).

Fig. 2 shows the *ab initio* points of Ref. 5 for three values of the θ angle, 0°, 45°, and 90°, in comparison with the analytical fit as expressed in Eq. (16).

III. RESULTS

The PIMC calculations performed at $T = 0.4$ K for the He_N–He^{*-} and He_N–He_2^{*-} clusters are presented separately in Secs. III A and III B, respectively.

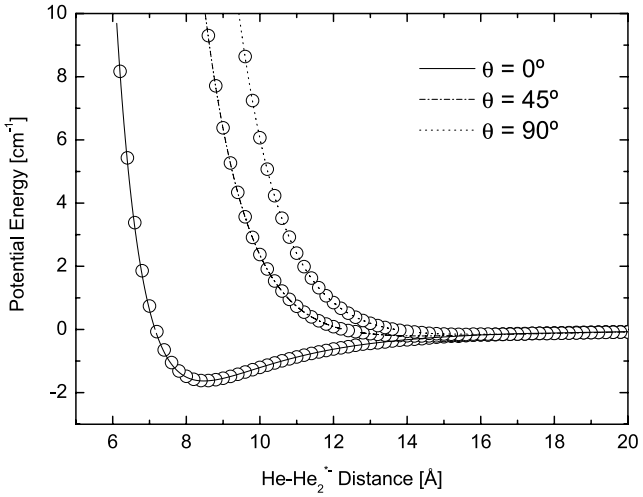

FIG. 2. Potential energy for the He–He_2^{*-} interaction for different values of the θ angle between each He atom and the CM of the He_2^{*-} impurity. Points are *ab initio* results from Ref. 5 and lines correspond to the fit by means of Eq. (16). Units of energy are cm^{-1} and distances are measured in Å.

A. He_N–He^{*-}

The geometries obtained with the EA for the He_N–He^{*-} clusters, with $N = 2$–8 are shown in Fig. 3. The He atoms place themselves surrounding the impurity, which ends up completely solvated in the center of a bipyramid when $N = 6$. The successively added He atoms remain outside this structure at larger distances from the impurity. An example of this configuration once the bipyramid is formed is seen in Fig. 3 for $N = 8$, for which the two last He atoms sit independently of the central structure of six atoms around the He^{*-} impurity.

Values of the energies for these He_N–He^{*-} clusters, with N ranging from 1 to 32, are presented in Table III. The effect of this preference to form the above mentioned bipyramid as stable configuration is observed in the trend of the corresponding energies as the He atoms are added. Thus, the variation of the E_{EA} energies with each atom is certainly well marked when there are still not enough He atoms to form the bipyramid, with differences between consecutive He_N–He^{*-} and He_{N+1}–He^{*-} clusters that range between ∼17 000 cm^{-1} for $N = 1$ and ∼6300 cm^{-1} for $N = 5$. However, once the helium solvating cage is formed, the increase of the total energy with the inclusion of new He atoms reduces significantly: The energies of He_6–He^{*-} and He_7–He^{*-} differ only ∼4 cm^{-1}.

The EA explores the absolute minima of the PES and, in fact, the value of the energies for the smallest clusters is roughly equivalent to N times the He–He^{*-} potential minimum:

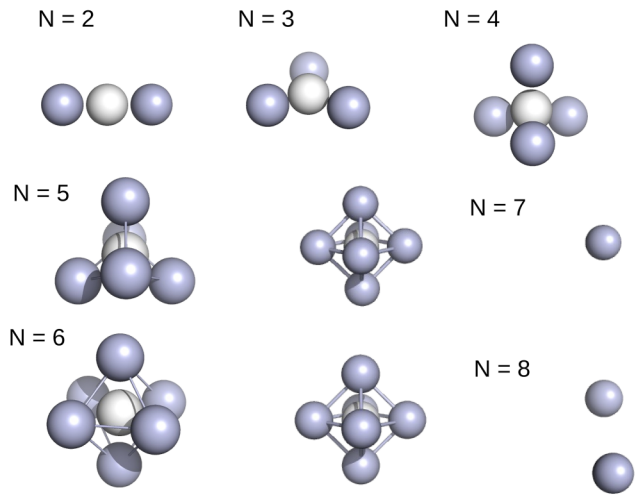

FIG. 3. Configurations obtained by means of the EA of Sec. II for He_N–He^{*-} clusters with $N = 2$–8.

TABLE III. Energies in cm^{-1} for the He_N–He^{*-} systems obtained by means of the PIMC approach (second column), its classical variant with $M = 1$, CMC (third column), and the corresponding EA values (fourth column) corresponding to the initial configurations of the MC simulation. Errors for the PIMC energies are in parentheses. See text for details.

N	PIMC	CMC	EA
1	−17 013.8 (28.0)	−17 169.0	−17 169.1
2	−33 707.0 (46.5)	−34 133.7	−34 134.6
3	−48 588.0 (126.1)	−49 207.8	−49 208.6
4	−61 342.0 (98.5)	−61 925.8	−61 927.1
5	−66 412.4 (268.3)	−67 685.0	−67 686.7
6	−72 378.7 (262.2)	−74 001.6	−74 003.8
7	−72 392.4 (267.6)	−74 005.9	−74 008.1
8	−72 385.5 (186.7)	−74 017.8	−74 012.0
16	−72 613.6 (206.0)	−74 246.7	−74 252.3
32	−72 988.5 (224.6)	−74 660.8	−74 601.3

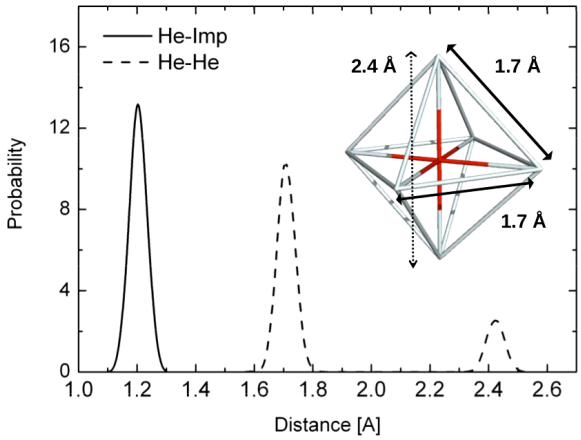

FIG. 4. Bipyramid structure for He_6–He^{*-} and radial probability distributions obtained with the PIMC calculation.

$E_{EA}^{(N)} \sim N \times V_{He-Imp}^{min}$. Although this trend is quickly abandoned (as shown in Table III for $N = 3$ the deviation is ∼2000 cm^{-1}), the formation of the bipyramid is directly related to this deep potential minimum in the helium-impurity interaction, a feature which the PIMC calculations confirm as we discuss below. For the largest clusters, once the vacancies surrounding the He^{*-} dopant according to the V_{He-Imp}^{min} value are occupied, the accessible minima are only those corresponding to the He–He interaction and the more swallow minimum of the He–impurity potential around $r_{He-Imp} \sim 7$ Å (see Fig. 1).

The values of the energies obtained by means of the PIMC at $T = 0.4$ K and the CMC version ($M = 1$) are also shown in Table III. The E_{CMC} energies are consistent with the previously analyzed E_{EA}, displaying the same trend as the He atoms are added to the cluster and remaining slightly above the EA results as a consequence of the existing dependence on T in the Metropolis procedure to search for the potential energy minimum within the CMC method. The only discrepancies with the expected comparison between the E_{CMC} and E_{EA} values are found for $N = 16$ and $N = 32$, two cases in which the predictions obtained by means of the EA are possibly subject to more marked uncertainties due to the difficulties to explore a reliable absolute minimum for large clusters once the solvating bipyramid has already been formed.

The values between parentheses for the E_{PIMC} in Table III correspond to the errors in the fitting procedure to a parabolic law to the $M \to \infty$ case. The comparison with the results from the other two classical approaches reveals the contribution to the total energy of the zero energy effect. Energies for He_6–He^{*-}, He_7–He^{*-}, and He_8–He^{*-} are quite similar, thus suggesting some sort of saturation when $N \gtrsim 6$. Present results also indicate the preference of the He atoms to occupy interparticle distances which are driven by the minimum of the He–He potential outside the bipyramid structure. In fact, although the associated errors are clearly larger than the actual differences among these three E_{PIMC} values, one might explain for instance the difference between the E_{PIMC} for He_6–He^{*-} and He_8–He^{*-}, ∼8 cm^{-1}, in terms of the $V_{He-He}(r_{min})$, considering the cluster with $N = 8$ as a bipyramid caging the impurity bond to an external He_2 unit such as He_6He^{*-}–He_2.

A detailed analysis of the geometry of the clusters has been performed by means of the corresponding density probability functions defined in Eqs. (6)–(8). In particular, in Fig. 4 we show the radial distributions corresponding to the He–He and He–impurity distances for the He_6–He^{*-} cluster obtained with the PIMC method at $T = 0.4$ K. As already found with the previous calculations of EA, the He atoms are located at the vertexes of a squared-basis bipyramid as shown in the snapshot of the MC simulation in Fig. 4. The maximum observed for the $\mathcal{D}_N(r_{He-He})$ distribution (see Eq. (6)) at $r_{He-He} \sim 1.7$ Å describes, on one hand, the He–He distances between atoms within the basis of this rigid structure and, on the other hand, the separation between any of those atoms and the upper/bottom vertices of the bipyramid. The other maximum, centered around $r_{He-He} \sim 2.4$ Å, corresponds in turn to the average distance between the He atoms located at the upper and bottom vertex and to the diagonal of the squared basis. Half a diagonal, ∼1.2 Å, is precisely the distance between the He atoms at the vertices of the square and the dopant He^{*-} at the center of the bipyramid and also the distance r_{He-imp} between the impurity and the upper and bottom He in the bipyramid. The maximum of the $\mathcal{D}_N(r_{He-imp})$ probability density distribution (see Eq. (7)) is located at such a value of r_{He-imp}, which on the other hand is not far from ∼1.07 Å, the distance for the minimum in the He–impurity potential as shown in Fig. 1.

Further support for the existence of this rigid central geometry found for the six first He atoms surrounding the dopant He^{*-} is given by the angular $\mathcal{D}_N(\cos\gamma)$ distribution (see Eq. (8)) for the He_6–He^{*-} system shown in Fig. 5. Clear peaks at $\cos\gamma \sim -1$ and 0 testify to the occurrence of 180° and 90°, the only two possible values for the angle formed by the position vectors of each pair of He atoms in the structure shown in Fig. 4. Signatures of such maxima are also clearly manifested in the corresponding angular distributions for larger He_N–He^{*-} systems. Fig. 5, for example, shows $\mathcal{D}_{32}(\cos\gamma)$, the probability density for $N = 32$ in comparison with the distribution for $N = 6$. The presence of these two peaks in combination with a broad background population can be explained in terms of the existence of the bipyramid besides the surrounding He atoms. The almost negligible

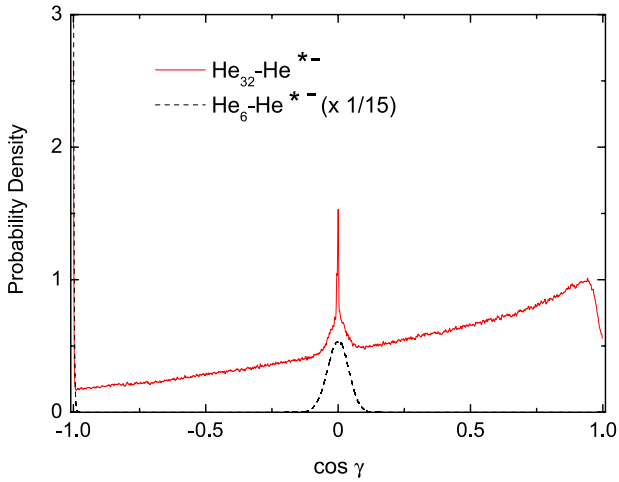

FIG. 5. Probability density distribution for $\cos\gamma$ defined in Eq. (8) for the He_6–He^{*-} and He_{32}–He^{*-} clusters at $T = 0.4$ K. Results for N = 6 are divided by 15.

population at $-1 \lesssim \cos\gamma \lesssim -0.1$, apart from the features due to the bipyramid, suggests that the dopant is not completely solvated but placed inside a broad dimple.

Snapshots taken from the MC simulation confirm this hypothesis. In Fig. 6, the structure for the He_{32}–He^{*-} cluster in a PIMC calculation at $T = 0.4$ K with $M = 100$ shows the He^{*-} impurity inside a six-He-atom cage and the surrounding helium environment formed by the remaining twenty-six solvating atoms. As suggested above from the EA results (see Fig. 1) for $N = 8$, the He atoms added to the system once the sites at the bipyramid are occupied, become located at one side of this central structure without covering it completely.

The mobility of the He atoms has to be necessarily different in the first shell formed by the closest bipyramid compared with those belonging to the more external helium cloud. The six He atoms in the vicinity of the He^{*-} dopant occupy almost fixed positions in the vertices of the central more rigid solvating structure with no capability to move. The corresponding M beads associated to these central He atoms hardly change and in fact look like a unique bead during the entire simulation. The polymers of beads in the PIMC describing the remaining

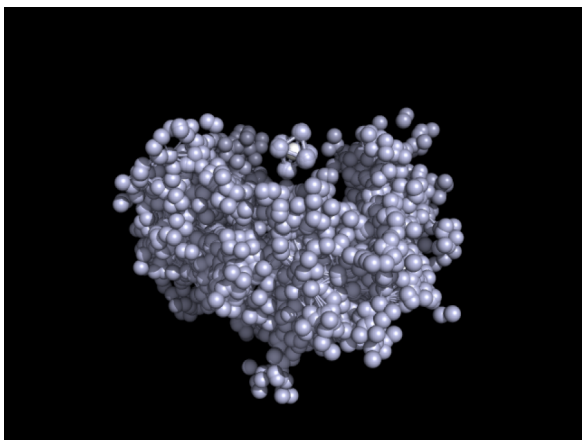

FIG. 6. Snapshot from the PIMC simulation for the He_{32}–He^{*-} cluster at $T = 0.4$ K. Lines connecting the He atoms of the bipyramid are plotted to remark the existence of such structure surrounding the impurity.

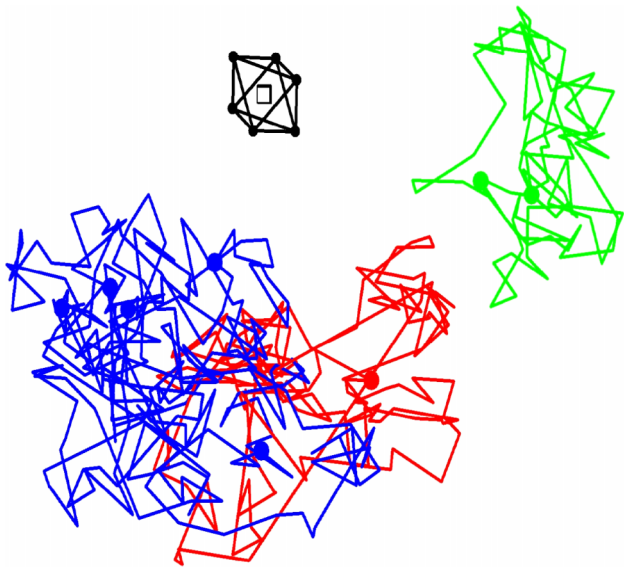

FIG. 7. Snapshot from the PIMC simulation for He_{16}–He^{*-} cluster at $T = 0.4$ K with cycles formed with the path chains of He atoms taking part in exchange permutation of two (green), three (red), or five (blue) He atoms.

atoms extend on the contrary over a much broader region. We have found that these external He atoms may participate in exchange movements according with the permutation Bose symmetry taken into account in the PIMC calculation for identical particles (see Eq. (3)). As shown in Fig. 7 for the case of the He_{16}–He^{*-} cluster, the remaining eight He atoms outside the bipyramid describe permutation cycles of different length. In particular, for the snapshot considered in this case, the closed polymers involve two (green), three (red), or five (blue) He atoms. Similar permutation movements have been seen for He_8–He^{*-}, but the occurrence of these exchanges is noticeably lower. The analysis in larger systems such as He_{32}–He^{*-} reveals that as expected the existence of long cycles becomes more probable when the size of the doped clusters increases.

B. He_N–He_2^{*-}

As for the case of the atomic anion, PIMC simulations for the He clusters doped with the diatomic impurity He_2^{*-} also start from optimized configurations obtained after a combined application of the EA and CMC approaches outlined before. The energies of the He_N–He_2^{*-} clusters with $N = 6$, 8, and 10 calculated with this approach are compared with the CMC and PIMC results in Table IV. The values predicted by the EA indicate that the total minimum of the PES is affected by the difference between the well depths of the He–He and He–He_2^{*-} potentials: ~7.9 cm^{-1} and ~2 cm^{-1}, respectively. The location of the He atoms within the pure helium droplet seems to respond primarily to the equilibrium distance of the $V_{He–He}$ potential. Thus, the $E_{EA}^{(N)}$ values can be roughly explained with binding energies of He–He pairs inside the cluster (see Table IV): For $N = 6$, the corresponding energy, -98.765 cm^{-1}, is approximately the result of about twelve pairs of He atoms separated about ~3 Å; $E_{EA}^{(8)}$ is almost nineteen He–He pairs at their equilibrium distance and $E_{EA}^{(10)}$ can be approximated

TABLE IV. Energies in cm^{-1} for the He_N–He_2^{*-} clusters obtained by means of the PIMC approach at $T = 0.4$ K (second column), the CMC (third column), and the EA (fourth column) corresponding to the initial configurations of the MC simulation. Values from VMC and DMC calculations of Ref. 27 for pure helium He_N clusters are included for comparison (fifth and sixth columns). Errors for the PIMC energies are given in parentheses.

N	PIMC	CMC	EA	He_N (VMC)[27]	He_N (DMC)[27]
6	−3.350 (0.365)	−96.429	−98.765	−1.533	−1.647
8	−4.092 (0.324)	−153.430	−156.248	−3.262	−3.568
10	−6.775 (0.229)	−217.905	−220.485	−5.502	−6.015

as $\sim 26 \times V_{\mathrm{He-He}}(r_{\mathrm{min}})$. In all cases, the remaining He atoms maintain interparticle distances of ∼4.8 Å, which, for example, for the He_6–He_2^{*-} cluster, is nearly describing a quadrangular bipyramid.

As observed for the He^{*-}-doped clusters, the predictions obtained with the CMC are consistent with the EA results, with differences of about 5–8 cm^{-1}. The PIMC for the $T = 0.4$ K, on the contrary, yields to significantly weaker bound states for the three $N = 6$, 8, and 10 cases. The values in parentheses in the second column of Table IV correspond to the errors in the fitting of the PIMC energies to a quadratic law in terms of $1/M$ to extrapolate the value for $M \to \infty$. The resulting E_{PIMC} obtained for the He_N–He_2^{*-} clusters can be compared with the corresponding energies for the pure He_N droplets. Also included in Table IV, values for He_6, He_8, and He_{10}, from the variational MC (VMC) and diffusion MC (DMC) calculations performed by Ref. 27 can give an idea of the stability of the doped clusters. It is worth noticing that the comparison with results reported by Lewerenz may also be affected by the $T = 0$ character of the VMC and DMC approaches and the different version of the He–He potential employed in their work. Qualitatively speaking, Table IV suggest that, despite differences not being large, the He droplets manage to bind the He_2^{*-} impurity in a stable configuration. The weak He–impurity interaction seems to be capable to guarantee binding energies between 0.5-0.7 cm^{-1} (for the case of He_8–He_2^{*-} and He_{10}–He_2^{*-}) and ∼2 cm^{-1} for the smallest droplet with $N = 6$ He atoms.

The apparently small binding energies of the doped clusters are accompanied by the location of the He_2^{*-} dopant relatively far from the core formed by the He atoms. As shown in the snapshot of the PIMC simulation for He_8–He_2^{*-} at $T = 0.4$ K of Fig. 8, the He droplets are found to be placed independently along the axis direction of the impurity. A stronger confirmation of this structure is obtained from the angular distributions for $\cos\gamma$ and $\cos\theta$ (see Eqs. (8) and (9), respectively) where the information refers to the average behaviour, not to a specific instant of the MC simulation. Fig. 9 shows how both $\mathcal{D}_8(\cos\gamma)$ and $\mathcal{D}_8(\cos\theta)$ for the doped cluster of $N = 8$ He atoms, peak close to 1. In the case of γ, values close to ≈0° are indications of proximity between the He atoms, a consistent feature with the more external He droplets shown in Fig. 8. In turn, $\theta \sim 0$ corresponds to the alignment of this helium cloud along the He_2^{*-} diatom axis, as expected from the minimum of the He–impurity interaction potential (see Fig. 2). This preference of the He atoms with respect to the dopant extends to the completely symmetric situation $\theta \sim 180°$.

Additional insight regarding the structure of the cluster is obtained via the radial probability density functions defined in Eqs. (6) and (7). In Fig. 10, we show the corresponding $\mathcal{D}_8(r_{\mathrm{He-He}})$ and $\mathcal{D}_8(r_{\mathrm{He-Imp}})$ distributions together with the probability density for the distance between each He atom and the CM of the He droplet calculated in a similar way, for He_8–He_2^{*-} at $T = 0.4$ K. According to the figure, the He atoms locate uniformly around the CM of the He_N structure with a maximum peak which in fact is not far from the equilibrium distance of the V_{HeHe} potential. This seems not to be the average distance found between He atoms as the maximum of $\mathcal{D}_8(r_{\mathrm{He-He}})$ is located beyond ∼2.9 Å extending up to noticeably larger values (∼12 Å). The distribution for $r_{\mathrm{He-Imp}}$ shows the preference of the impurity to be placed far from the He droplet. Interestingly, the $\mathcal{D}_8(r_{\mathrm{He-Imp}})$ function exhibits a maximum at slightly larger distances than the average

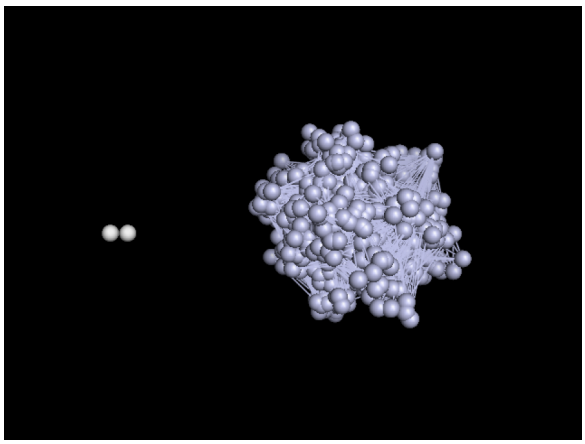

FIG. 8. Snapshot from the PIMC simulation for He_8–He_2^{*-} cluster at $T = 0.4$ K.

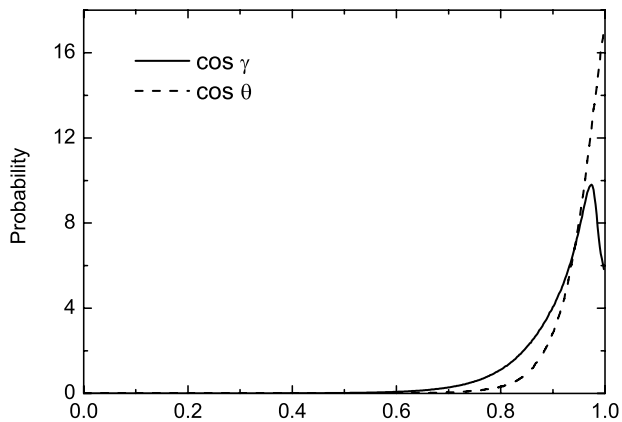

FIG. 9. Angular distributions $\mathcal{D}_N(\cos\theta)$ (dashed line) and $\mathcal{D}_N(\cos\gamma)$ (solid line) for He_8–He_2^{*-} cluster at $T = 0.4$ K.

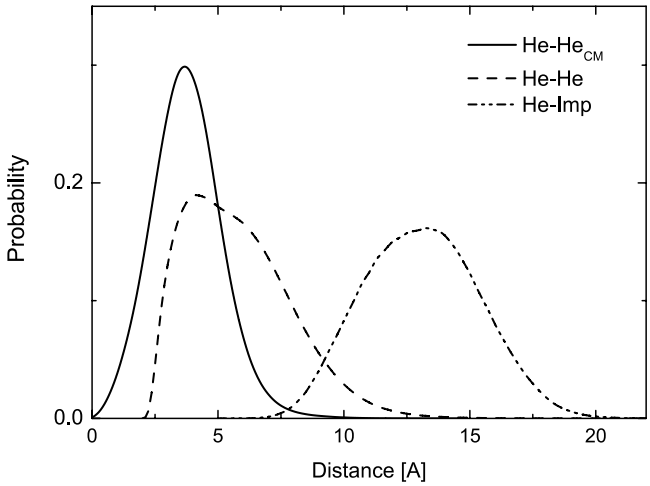

FIG. 10. Radial density distributions for He_8–He_2^{*-} cluster. Solid line is for the distance between the He atoms and the CM of the separate He_N droplet; dashed line for the He–He distance and dashed-dotted line is for the density for the distance between the He_2^{*-} impurity and the He atoms.

separation (between 9.5 and 12.5 Å) found by the EA in its search for the minimum energy configuration, thus suggesting that the PIMC calculation does not indicate any preference for the He–impurity distance to match the minimum according to the corresponding potential.

IV. DISCUSSION

As stated in Ref. 5, the He^{*-}–He system at the potential minimum (see Fig. 1) displays the structure of a He_2^+ core and a diffuse electronic shell due to the two electrons occupying σ and π orbitals. The bonds between the impurity and the atoms participating in the bipyramid structure seem to be the result of the polarization suffered by the tightly bound electrons of the He atoms due to the presence of the He_2^{*-} system. This inner solvating cage would be then formed by an ensemble of He^+ cations sharing an electronic cloud. This "chemically bound molecular" configuration existing at the shorter distances shifts, however, to a "polarisation-bound complex" at larger distances beyond the potential barrier exhibited by the He^{*-}–He potential around ~2.5 Å. Additional He atoms feel a much weaker potential due to the screening induced by the presence of the inner core of six atoms surrounding the impurity and move further out sampling the shallower local potential minimum located at ~7–8 Å.

The formation of a stable and rigid helium cage around the atomic anion is consistent with the previously suggested heliophilic character for He^{*-}.[2] One would have perhaps expected for it however a much clearer tendency to be completely solvated by the helium droplet in accord with the large mobility inside the cluster reported in previous studies. Present results indicate on the contrary that the dopant, once surrounded by the six-He-atom structure of a bipyramid, remains in a dimple formed in the outside of the largest calculated helium droplet. The explanation for this apparent separation between this rigid structure and the remaining He atoms can be found in the nature of the He–He^{*-} interaction. The solvating He atoms tend in general to establish a more stable interaction with the He fixed in the vertices of this bipyramid at ~2.8 Å, the He–He equilibrium distance according to the V_{He-He} potential. However, that would mean to be located at ~4.5 Å from the He^{*-} dopant in the center of the first-solvation-shell cage, a position which is prevented by the presence of the pronounced barrier at ~5 Å (see Fig. 1). Despite this safety distance which blocks the approach of He atoms more closely to the dopant, it is possible to also surmise that a larger number of He atoms could lead to the formation of a bubble-like structure around the He_6–He^{*-} inner core. In this sense, it is worth recalling situations where an almost complete solvation around the dopant has been observed with a similar number of He atoms. Thus, for example, the SF_6 molecule was found to be surrounded in all directions by only 23 He atoms[28] and, for He_N–Ca clusters,[12] $N = 40$ He atoms suffice to surround almost completely the Ca atom once a strong enough He–impurity interaction potential was employed. For the present case, the V_{He-Imp} potential, much more stronger than those considered by Rodríguez-Cantano *et al.* in Ref. 12, is responsible for the tight central geometry of a core formed by six He atoms which in fact screen the interaction with the rest of surrounding atoms thus preventing a complete solvation.

Previous studies on doped He clusters treated the analysis of the PIMC permutation cycles generated when the Bose symmetry of identical particles is properly taken into account to identify possible superfluid features of the system. In particular, the participation in exchange rings of certain length involving several He atoms has been employed to determine qualitatively the extent of the superfluid character.[29] Comparative investigations at $T = 1.25$ K and $T = 0.625$ K of the He_{29}–SF_6 cluster revealed that exchange effects were relevant at the lower temperature, whereas at $T = 1.25$ K long paths involving several permuting He atoms were not observed.[17] Analogously, the length of the exchange permutation paths was found to increase with the number of He atoms surrounding the SF_6 impurity. Thus, in their investigation on He_NSF_6 molecules at $T = 0.625$ K, Kwon *et al.*[28] obtained lengths for the permutation paths of up to seven exchanged He atoms for $N = 23$, a maximum number which increased up to 59 in the case of $N = 128$. In this sense, the case of He_N–He^{*-} here investigated presents some similarities regarding the existence of relatively long permutation PIMC paths both at low temperatures and when the number of solvating He atoms is increased.

The potential depth of the He–He_2^{*-} interaction is slightly smaller than those existing in other doped He clusters such as He_N–Rb_2[30,31] and He_N–Cs_2.[13,32] However, the main difference with these other two cases lies in the location of the minimum of the potential: whereas for the interaction with both Rb_2 and Cs_2, the He atoms find the most stable configuration at the T–shaped direction, $\theta \sim 90°$, for the molecular anion He_2^{*-}, the potential minimum of the He–impurity interaction is along the diatom axis, $\theta \sim 0°$. For clusters formed with stronger interactions, such as $HeBr_2$,[33] it is possible to find the contribution from both the T-shaped and linear He–impurity configurations. In addition, this preference for the linear direction observed in the He–He_2^{*-} potential is accompanied by the absence of any appreciable well at any other angular configuration (see Fig. 2). The PES for the He–Rb_2 and He–Cs_2 interaction, on the

contrary, displays relative minima over the entire angular range down to the linear geometry, thus offering stable alternative structures for the He atoms added to the impurity. The distance between the neutral He atom and the ionic dopant according to this minimum potential energy configuration is also larger, ~8.5 Å, than the values observed for the corresponding $He–Rb_2$ and $He–Cs_2$ separations of ~6.5–7 Å.[30,32] The dopants place themselves in all these cases outside the He droplet, thus indicating their heliophobic character, as opposed to some other clusters, such as $He_N–I_2$,[34] mediated by a much stronger He–impurity interaction in which the dopant is solvated within the He droplet.

Besides the results shown in Sec. III B, the PIMC calculations can yield configurations for the $He_N–He_2^{*-}$ clusters with the helium droplet at a slightly deviated direction of the He_2^{*-} diatom axis. This observed departure from the alignment with respect to the diatomic impurity would have an explanation if it could be linked to some sort of anisotropy induced by the PES, but this is not the situation found in the $He–He_2^{*-}$ interaction. The origin of this apparently anomalous behaviour is possibly related to deficiencies either on the *ab initio* points or the fitting procedure since the deviation is observed in the preliminary calculations performed with the EA in order to obtain initial configurations for the PIMC. The use of cutoff distances preventing the He atoms to locate too close to the impurity and limitations to the maximum value of the $V_{He–imp}$ in an attempt to control the location of the surrounding atoms did not avoid this apparently spurious result. Another possible explanation regards the above mentioned lack of secondary minima in the $He–He_2^{*-}$ interaction. The PIMC algorithm might find difficulties in such essentially flat potential landscapes whenever the EA employed to search for the minimum in the selection process of initial configurations for the MC simulation ends up sampling regions with the He atoms separated from the strict $\theta \sim 0°$ configuration.

V. CONCLUSIONS

The energetics and geometries of helium clusters He_N doped with He^{*-} and He_2^{*-} at $T = 0.4$ K have been investigated by means of a PIMC method. The interactions between the dopant and the helium atoms are described with an analytical fitting of previously reported *ab initio* points. The atomic anion is solvated by six He atoms forming a bipyramid structure which is located in a dimple partially surrounded by the remaining He droplet, a consistent finding with reported suggestions of a heliophilic and highly mobile impurity embedded in helium. The molecular anion formed $He_N–He_2^{*-}$ droplets with smaller binding energies in comparison with those corresponding pure He_N systems. The observed geometries indicate an outer location of the impurity with respect to the helium atoms in agreement with results for systems such a $He_N–Rb_2$ or $He_N–Cs_2$, mediated by similarly weak He–impurity interactions.

ACKNOWLEDGMENTS

This work has been supported by MICINN Grant No. FIS2011-29596-C02-01. R.R.-C. acknowledges funding from Grant No. JAE-Pre-2010-01277. F.A.G. acknowledges several helpful discussions with A. Mauracher and thanks him for providing us with the original computed *ab initio* points for the He–dopant interactions.

[1]U. Henne and J. P. Toennies, J. Chem. Phys. **108**, 9327 (1998).
[2]A. Mauracher, M. Daxner, J. Postler, S. E. Huber, S. Denifl, P. Scheier, and J. P. Toennies, J. Phys. Chem. Lett. **5**, 2444 (2014).
[3]S. E. Huber and A. Mauracher, J. Phys. Chem. A **118**, 6642 (2014).
[4]K. Martini, J. Toennies, and C. Winkler, Chem. Phys. Lett. **178**, 429 (1991).
[5]S. E. Huber and A. Mauracher, Mol. Phys. **112**, 794 (2014).
[6]C. G. Kuper, Phys. Rev. **122**, 1007 (1961).
[7]J. Poitrenaud and F. I. B. Williams, Phys. Rev. Lett. **29**, 1230 (1972).
[8]G. G. Ihas and T. M. Sanders, Phys. Rev. Lett. **27**, 383 (1971).
[9]S. Denifl, F. Zappa, I. Mähr, J. Lecointre, M. Probst, T. D. Märk, and P. Scheier, Phys. Rev. Lett. **97**, 043201 (2006).
[10]J. Postler, V. Vizcaino, S. Denifl, F. Zappa, S. Ralser, M. Daxner, E. Illenberger, and P. Scheier, J. Phys. Chem. A **118**, 6553 (2014).
[11]L. Adamowicz and T. Pluta, Phys. Rev. A **44**, 2860 (1991).
[12]R. Rodríguez-Cantano, T. González-Lezana, P. Villarreal, D. López-Durán, F. A. Gianturco, and G. Delgado-Barrio, Int. J. Quantum Chem. **114**, 1318 (2014).
[13]R. Pérez de Tudela, D. López-Durán, T. González-Lezana, G. Delgado-Barrio, P. Villarreal, F. A. Gianturco, and E. Yurtsever, J. Phys. Chem. A **115**, 6892 (2011).
[14]R. Rodríguez-Cantano, D. López-Durán, R. Pérez de Tudela, T. González-Lezana, G. Delgado-Barrio, P. Villarreal, and F. A. Gianturco, Comput. Theor. Chem. **990**, 106 (2012).
[15]R. Rodríguez-Cantano, R. Pérez de Tudela, D. López-Durán, T. González-Lezana, F. A. Gianturco, G. Delgado-Barrio, and P. Villarreal, Eur. Phys. J. D **67**, 119 (2013).
[16]D. M. Ceperley, Rev. Mod. Phys. **67**, 279 (1995).
[17]Y. Kwon, D. M. Ceperley, and K. B. Whaley, J. Chem. Phys. **104**, 2341 (1996).
[18]R. Pérez de Tudela, M. Marquez-Mijares, T. González-Lezana, O. Roncero, S. Miret-Artés, G. Delgado-Barrio, and P. Villarreal, J. Chem. Phys. **132**, 244303 (2010).
[19]D. M. Ceperley and E. L. Pollock, Phys. Rev. Lett. **56**, 351 (1986).
[20]D. M. Ceperley and E. L. Pollock, Phys. Rev. B **39**, 2084 (1989).
[21]Y. K. P. Huang and K. B. Whaley, *Microscopic Approaches to Quantum Liquids in Confined Geometries*, Series on Advanced in Quantum Many-Body Theory Vol. 4, edited by E. Krotscheck and J. Navarro (World Scientific, 2002), p. 91.
[22]J. A. Barker, J. Chem. Phys. **70**, 2914 (1979).
[23]J. E. Cuervo and P.-N. Roy, J. Chem. Phys. **125**, 124314 (2006).
[24]N. Blinov, X. Song, and P.-N. Roy, J. Chem. Phys. **120**, 5916 (2004).
[25]M. Iwamatsu, Comput. Phys. Commun. **142**, 214 (2001).
[26]R. A. Aziz and M. J. Slaman, J. Chem. Phys. **94**, 8047 (1991).
[27]M. Lewerenz, J. Chem. Phys. **106**, 4596 (1997).
[28]Y. Kwon, P. Huang, M. V. Patel, D. Blume, and K. B. Whaley, J. Chem. Phys. **113**, 6469 (2000).
[29]E. L. Pollock and D. M. Ceperley, Phys. Rev. B **36**, 8343 (1987).
[30]R. Rodríguez-Cantano, D. López-Durán, T. González-Lezana, G. Delgado-Barrio, P. Villarreal, E. Yurtsever, and F. A. Gianturco, J. Phys. Chem. A **116**, 2394 (2012).
[31]G. Guillon, A. Zanchet, M. Leino, A. Viel, and R. E. Zillich, J. Phys. Chem. A **115**, 6918 (2011).
[32]R. Prosmiti, G. Delgado-Barrio, P. Villarreal, E. Yurtsever, E. Coccia, and F. A. Gianturco, J. Phys. Chem. A **113**, 14718 (2009).
[33]M. I. Hernández, T. González-Lezana, G. Delgado-Barrio, P. Villarreal, and A. A. Buchachenko, J. Chem. Phys. **113**, 4620 (2000).
[34]R. Pérez de Tudela, P. Barragán, A. Valdés, and R. Prosmiti, J. Phys. Chem. A **118**, 6492 (2014).